Printable homocomposite hydrogels with synergistically reinforced molecular-colloidal networks

Austin Williams
North Carolina State University
Sangchul Roh
North Carolina State University
Alan Jacob
North Carolina State University
Simeon Stoyanov
Wageningen University
Lilian Hsiao
North Carolina State University https://orcid.org/0000-0002-4448-7397
Orlin Velev (odvelev@ncsu.edu)
North Carolina State University https://orcid.org/0000-0003-0473-8056

Article

Keywords: homocomposite hydrogels, soft dendritic colloids, 3D printing

Posted Date: December 2nd, 2020

DOI: https://doi.org/10.21203/rs.3.rs-110699/v1

Version of Record: A version of this preprint was published at Nature Communications on May 14th, 2021. See the published version at https://doi.org/10.1038/s41467-021-23098-9.

Printable homocomposite hydrogels with synergistically reinforced molecular-colloidal networks

Austin H. Williams[‡1], Sangchul Roh[‡1], Alan R. Jacob[1], Simeon D. Stoyanov[1,2,3], Lilian Hsiao[1], and Orlin D. Velev[1*]

[1] Department of Chemical and Biomolecular Engineering, North Carolina State University, Raleigh, NC 27695, USA.

[2] Physical Chemistry and Soft Matter, Wageningen University, The Netherlands.

[3] Department of Mechanical Engineering, University College London, Torrington Place, London WC1E 7JE, UK.

[‡] *These authors contributed equally to this work*

* *Corresponding author. E-mail: odvelev@ncsu.edu*

Submitted to Nature Communications, Nov. 17, 2020.

The design of hydrogels where multiple interpenetrating networks enable enhanced mechanical properties could benefit applications such as biomedical products, 3D printing, and soft robotics. We report a class of self-reinforced homocomposite hydrogels (HHGs) comprised of interpenetrating networks of multiscale hierarchy. A molecular alginate gel is reinforced by a colloidal network of hierarchically branched soft dendritic colloids (SDCs), which are also made of alginate. The reinforcement of the molecular gel with the nanofibrillar SDC network of the same biopolymer results in a remarkable increase of the HHG mechanical properties. The viscoelastic HHGs show >3× larger storage modulus and >4× larger Young's modulus than either constitutive network at the same concentration. Such synergistically enforced colloidal-molecular HHGs open numerous opportunities for formulation of biocompatible gels with robust structure-property relationships. Balance of the ratio of their precursors facilitates precise control of the yield stress and rate of self-reinforcement, enabling HHG 3D printing by extrusion.

Introduction

Hydrogels made of polymer networks in water are generally soft and fragile, often lacking the resilience and toughness required for widespread deployment in applications such as tissue scaffolds, food products, soft robotics, and flexible electronics[1–10]. The elasticity of these materials can be improved by combining interpenetrating covalent and ionic polymer networks to form highly stretchable and tough hydrogels[11–17]. Another way of improving and enhancing the mechanical properties of hydrogels is by including high aspect ratio fillers, such as fibers, to mechanically reinforce the gel matrix[18–26]. Fiber-reinforced hydrogels can serve as comprehensive bioscaffolds for cell growth. The fiber networks offer robust control of hydrogel stiffness, and can mimic the morphology of the physiological extracellular matrix, which has been shown to affect cell activity, differentiation and response[27,28]. Controlling hydrogel stress propagation by fiber reinforcement is also useful in applications such as soft robotics, as it may enable nonlinear deformation modes and durability against frictional sliding[29]. However, using fillers made of a different material from the matrix introduces stressed interfaces that cause crack formation when the composite hydrogels are strained or heated.

One different materials design approach is to use single-polymer composites, or so-called “homocomposites”. The mesoscale reinforcement network of homocomposites is made of a material that is chemically identical to that of the primary matrix. Homocomposite reinforcement networks allow modulation of the mechanical properties of the host matrix without stress concentrations, delamination points or other problems arising from interfacial incompatibilities[30,31]. Homocomposite formulations can also include liquid bridges as precursor binder in multiphasic silicone pastes used in 3D printing[32,33]. The chemical similarity of the continuous and reinforcement phases provides superior adhesion and enhanced load transfer[25,34–36]. Previous studies have also shown that homocomposites with fiber reinforcements allow tailored bulk melt rheology along with increased tensile modulus

and strength[37,38]. They are made by using the differences in melting temperatures between thermoplastic polymer crystalline phases as a processing window[39,40]. However, homocomposite hydrogels (HHGs) remain challenging to fabricate because of the lack of techniques to construct reinforcing networks with the same chemical composition as the hydrogel matrix.

We report a class of HHGs where both the primary gel matrix and the reinforcement network are made of sodium alginate (SA). Alginate hydrogels are used in a broad range of technological applications such as biomedical implants, tissue engineering scaffolds, and food products[7]. These HHGs are reinforced by a fibrillar network of alginate soft dendritic colloids (SDCs). The SDCs are a hierarchically structured class of soft matter synthesized through a scalable process of shear-driven precipitation in a turbulent medium, described in our recent report[41]. The high degree of branching around the cores of the SDC particulates makes them morphologically similar to polymeric molecular dendrimers, but SDCs are orders of magnitude larger than these dendrimers[42,43]. Our previous studies with polymer SDCs dispersed in an organic oil medium showed that the branched, nanofibrous structure of the dendricolloids enables efficient network formation leading to gelation at low volume fraction due to enhanced van der Waals interactions[41,44].

The hierarchically branched SDCs are expected to serve as efficient reinforcement in composite materials. Their branches provide large surface area, which could increase the composite stability by distributing the stress more uniformly[41,45–49]. We investigate here the SDC effectiveness in reinforcing homocomposite hydrogels, expecting that the high surface area and maximized adhesivity between the SDC network and the matrix will result in hydrogels of outstanding mechanical properties. To analyze the unusual mechanical properties of the HHGs, we also perform shear and tensile tests on their constituents: aqueous SA SDC suspensions and crosslinked SA molecular hydrogels (CMHs). We then characterize HHGs composed of SA SDCs embedded in a SA CMH matrix and discuss the origins of their

synergistically enhanced viscoelastic properties. On this basis, we demonstrate that the HHGs can be readily formulated to provide a yield stress for 3D printing or pressure-driven extrusion.

Results

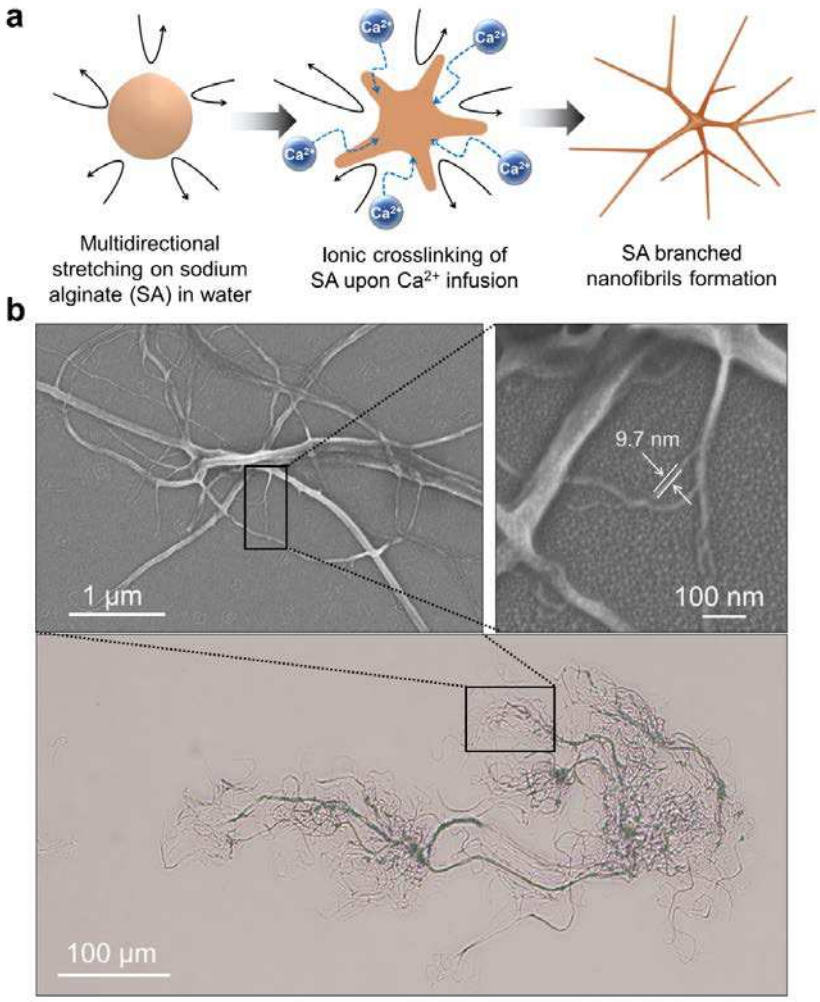

Fig.1 | Turbulent shear-driven precipitation and morphology of a sodium alginate soft dendritic colloid. a Schematic of the SA SDC formation process by precipitation in a turbulent medium. **b** Optical microscopy and field emission scanning electron microscopy (FE-SEM) images of sodium alginate soft dendritic colloids. These images illustrate the hierarchical fibrillar morphology of the SDCs, which leads to high exclusion volume, strong van der Waals adhesivity and high propensity for gelation.

Formation of soft dendritic colloids from alginate. The alginate SDCs used as reinforcement networks were fabricated using a turbulent shear-driven precipitation process

for the manufacturing of polymer dendricolloids[41]. In order to obtain hydrogel SDCs, a solution of alginate (120 – 190 kDa) was injected in an aqueous solution of Ca^{2+} ions, which effectively bind and crosslink two -COO- side groups on the alginate backbone (Fig. 1a). The turbulent shear precipitation process results in SDCs with characteristic hierarchical morphology, shown in Fig. 1b, with multiscale branching and generations of fibers spanning roughly 3 orders of magnitude in length scale. The SDCs are surrounded by coronas of nanofibers as thin as 10 nm in diameter. The SA SDCs suspensions were washed with deionized water to remove excess $CaCl_2$ ions from the suspension.

Viscoelastic properties of aqueous SDC suspensions. We first established whether alginate SDCs form colloidal network hydrogels at low volume fractions in water. The hypothesis is that in aqueous suspensions, SDCs will adhere strongly to one another through van der Waals forces to form a percolating network of branched fiber sub-contacts (Fig. 2a)[41]. Characterization of the storage (G') and viscous (G") moduli of SDC suspensions within the linear viscoelastic region using a stress-controlled rheometer showed that the SDCs have a strong propensity for forming colloidal networks. A yield stress was observed in aqueous suspensions of 0.25 wt.% SDCs, i.e., at a lower concentration than most types of conventional colloidal gels (Supplementary Fig. 1)[50]. The slopes of G' and G" obtained from small amplitude oscillatory frequency sweeps showed that SDC suspensions with solid content above 0.4 wt.% are gel-like in nature (Fig. 2b)[51–53].

The efficient networking of SDCs is likely a result of the abundant adhesive physical contacts between the flexible, branched dendricolloids[41], a phenomenon known as contact splitting that is responsible for the universal adhesivity of the footpads of gecko lizards[54]. SDC suspensions exhibit more pronounced solid-like characteristics than suspensions of common alginate particles. A 1.0 wt.% SDC suspension has a value of $G' \approx 200$ Pa as

compared to reported values of $G' = 10 - 100$ Pa for 1.0 wt.% alginate microgel suspensions[55–57].

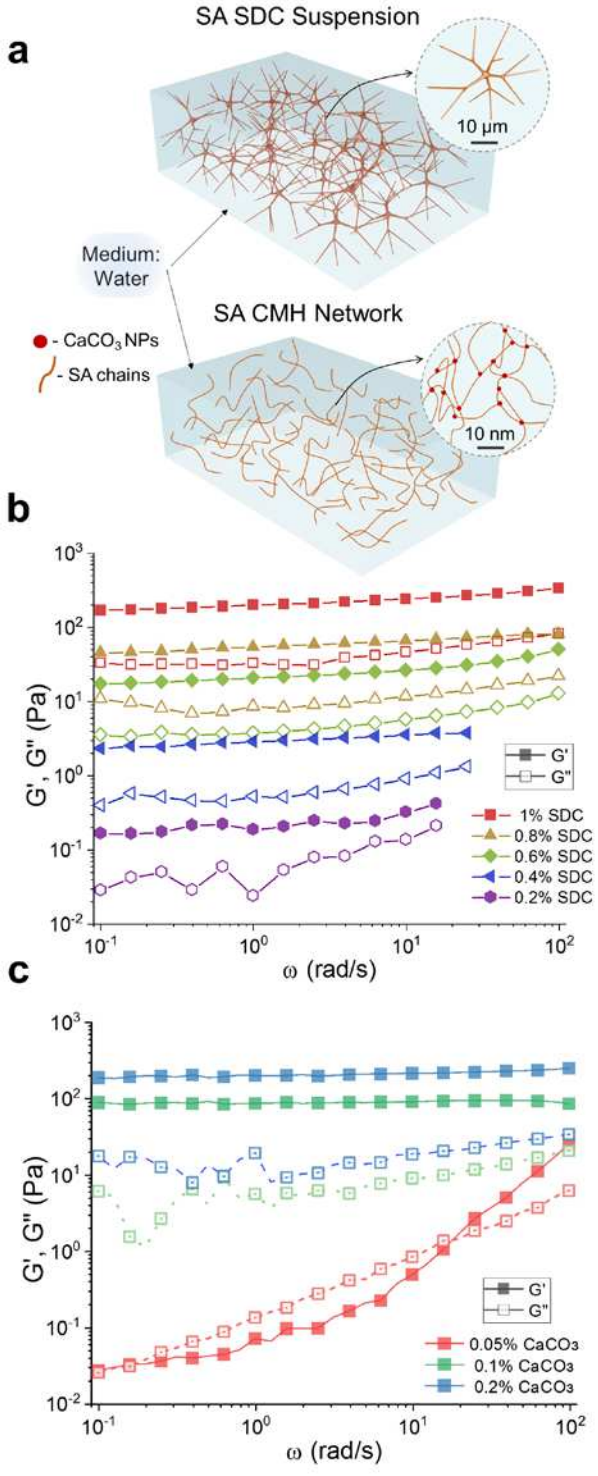

Figure 2 | Linear viscoelasticity and yield stress of SA SDC suspensions and molecular gels. **a** Schematic that compares the gelation mode of a viscoelastic suspension of SDCs and that of a crosslinked SA molecular hydrogel (CMH). Note the different length scales of the networks. **b** Frequency sweeps indicating the storage modulus (G', filled) and loss modulus (G″, unfilled) of SA SDCs in aqueous suspensions. **c** Frequency sweeps indicating the storage modulus (G', filled) and loss modulus (G″, unfilled) of 1.0% SA CMHs with 0.05%, 0.1% and 0.2% $CaCO_3$ nanoparticles and 28.14 mM GDL following 2 hours for equilibration.

Viscoelastic properties of alginate crosslinked molecular hydrogels (CMHs). The continuous phase of the HHGs consists of a molecular alginate crosslinked with Ca^{2+} ions. We first characterized the properties of molecular hydrogels made of 1.0 wt.% crosslinked alginate in the absence of SDCs. The CMHs were prepared by the addition of $CaCO_3$ nanoparticles and D-Gluconic acid δ-lactone (GDL) to a SA solution. As GDL undergoes hydrolysis and lowers the pH, the $CaCO_3$ slowly releases Ca^{2+} ions[58,59]. The linear viscoelastic properties of the CMHs following 2 hours of equilibration are plotted in Fig. 2c. Solid-like behavior is observed above 0.05 wt.% $CaCO_3$ (20/1 SA/$CaCO_3$). Further loading of the alginate hydrogel with Ca^{2+} increases its stiffness, however, we found that hydrogels containing $\geq$ 0.2 wt.% $CaCO_3$ (5/1 SA/$CaCO_3$) exhibited significant syneresis – pronounced shrinkage of the crosslinked gel accompanied by release of water (Supplementary Fig. 2). To avoid syneresis, we worked further with CMHs of 10/1 SA/$CaCO_3$ ratio. Interestingly, at this ratio the pure CMH and SDC gels of 1.0 wt.% had storage moduli of similar magnitude, even though these two systems are gelled by different physical mechanisms and are very dissimilar in their appearance (clear CMH gels vs. turbid SDCs suspensions).

Viscoelastic properties of composite HHGs. We next investigated how the colloidal network of SA SDCs can be combined with the molecular SA CMH matrix and crosslinked to produce self-reinforced HHGs. We synthesized a variety of HHGs where the total SA concentration was kept constant at 1 wt.% while the ratio of SDCs to CMH was varied (Table 1). The G' and G" values of the HHGs were measured as a function of time using small amplitude oscillatory stress and frequency sweeps after an equilibration time of t = 2 h. All HHG samples exhibited solid-like behavior (Fig. 3a). Notably, the G' values of all HHG samples were larger than those of either pure CMHs or pure SDC suspensions, with maximum values recorded at low SDC concentrations (0.175 – 0.25 wt.% SDCs). Representative stress-

strain curves (Fig. 3b) obtained by mechanical tensile testing also demonstrate that the HHG systems have larger stiffness than the gels from SDCs or CMHs alone.

The data from both rheometry and tensile stress-strain measurements for all HHGs are consolidated in Fig. 3c. These data demonstrate that the homocomposite systems comprising mixed SDCs and CMHs exhibit a strong synergistic effect. Both the values of the complex modulus G^*, and the Young's modulus, E, for the homocomposite gels showed greater than 3× increases with maxima at low SDCs to CMH ratios. This effect cannot be solely attributed to the slightly increased concentration of the Ca^{2+} crosslinker in the homocomposite system with Ca^{2+} localized both within the SDC reinforcement as well as homogenously distributed through the CMH continuous phase. The highest shear modulus measured in HHGs (G^* = 950 Pa at a composition of 0.125% SDCs/0.875% CMH) does not correspond to the highest Ca^{2+} concentration, as further increasing the SDC content reduces the resulting HHG stiffness. The Ca^{2+} concentration in this formulation was estimated to be ~ 1.5× the concentration found in the pure CMH (Supplementary Fig. 3, Supplementary Table 1). A frequency sweep performed on a CMH with 2× $CaCO_3$ shows that the $G^* \approx 250$ Pa (Fig. 2c), which is much less than that of the stiffest HHG formulation (0.125% SDCs/0.875% CMH). Thus, the strong synergistic effect leading to increased mechanical strength of the HHGs is directly attributed to the physical entanglement of the molecular SA and colloidal SDC networks, where the divalent Ca^{2+} ions bridge the alginate chains at the interface between the microgel fibers and the continuous matrix[57]. The resulting HHG structure is illustrated in Fig. 3d.

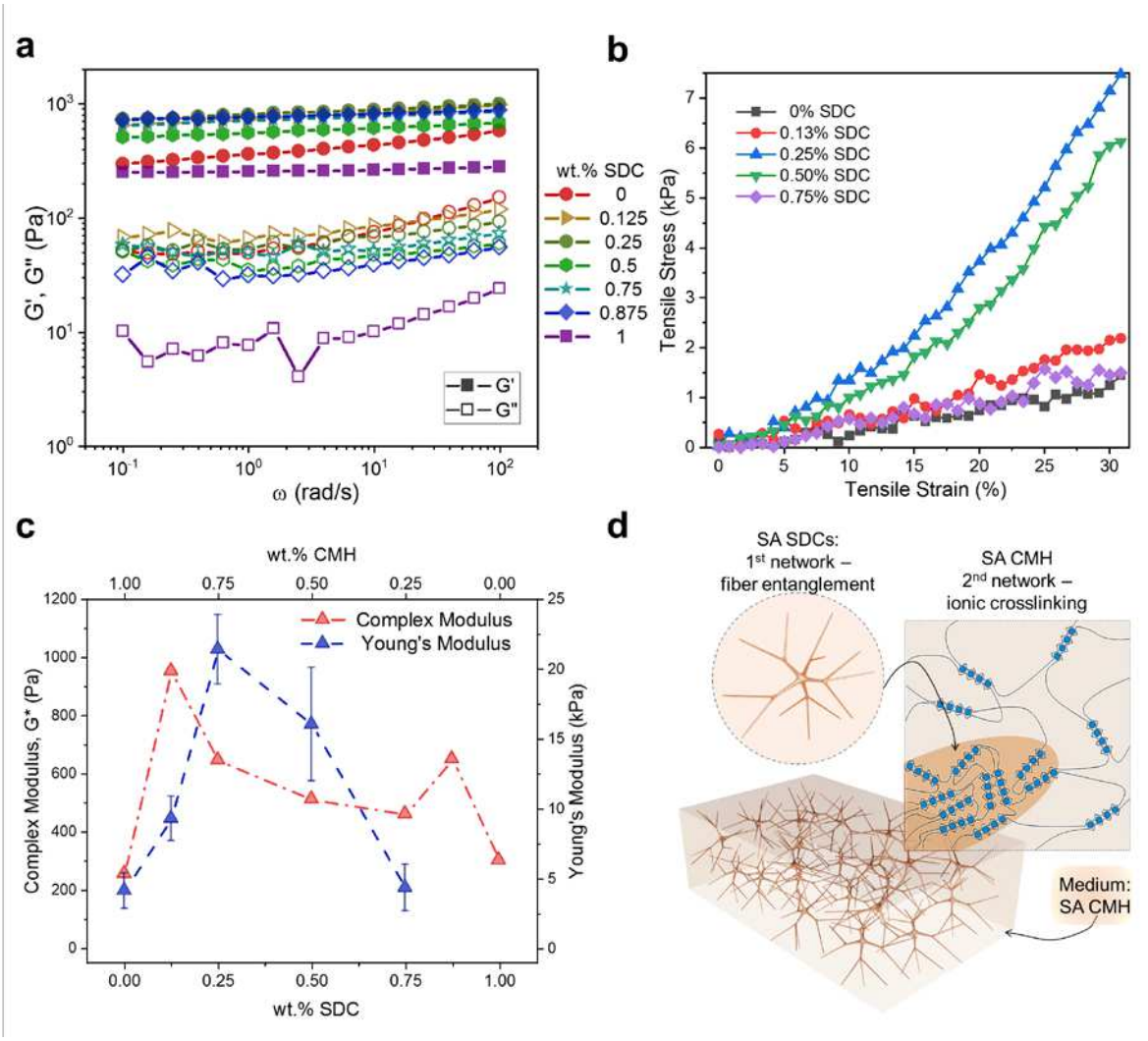

Figure 3 | Mechanical properties of SA homocomposite gels. a Frequency sweeps of 1.0% HHGs of varying SDC concentrations (n=2). **b** Representative stress-strain curves for various HHGs. **c** Rheological (□, n=2) and tensile (▲, n=5) properties of various SDC/CMH HHGs. Total alginate concentration is maintained at 1.0 wt.% for all data. **d** Schematic of the hierarchical interactions between the colloidal and molecular alginate networks in HHGs. These results demonstrate the structural synergism of the double SDC and CMH networks within HHGs resulting in controllable and self-reinforced high composite stiffness.

Time-dependent stiffening of homocomposite hydrogels. One of the other functionalities imparted by the colloidal-molecular networks in the HHGs is in the tunability of their gelation kinetics. We measured the time dependence of gelation through oscillatory shear rheology performed on SDCs, CMHs, and composite HHGs at the same SA concentration of 1 wt.%. The time sweeps performed with a pure 1 wt.% SDC suspension plotted in Fig. 4a show that the SDC suspension immediately exhibits solid-like behavior without the addition of $CaCO_3$ or GDL. This is expected, as the formation of this network occurs by contact splitting and

entanglement of the fibrillar dendricolloids. The values of G' and G'' of this system do not show any further stiffening by crosslinking or densification. The pure CMH, on the other hand, initially shows liquid-like behavior and gradually solidifies as Ca^{2+} crosslinker is released by hydrolysis. It develops into a fully crosslinked system in ≈ 120 mins (Fig. 4b).

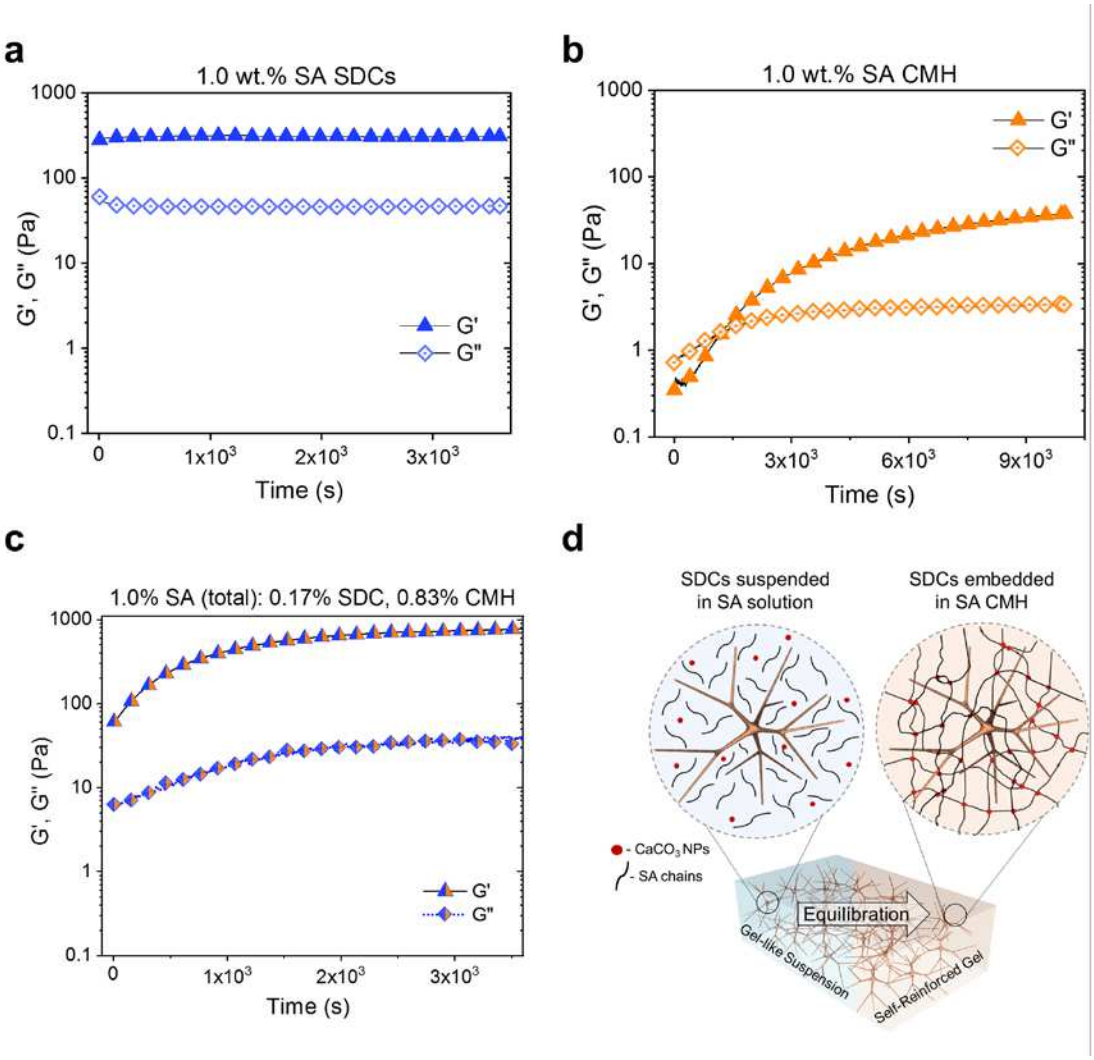

Figure 4 | Time-dependent gelation of SA SDC suspensions, SA CMHs, and SA HHGs. Time sweeps indicating G' and G'' (1 rad/s, 1% strain) of **a** 1.0 % SA SDC suspension in water, **b** 1.0% SA CMH following GDL addition and **c** 1.0% total SA (0.17% SDC, 0.83% CMH) HHG following GDL addition. **d** Schematic showing the time-dependent transition of a HHG from a colloidal gel to a self-reinforced homocomposite via CMH crosslinking. HHG formulations show immediate, elastic-solid behavior from the colloidal network and further stiffen with the ionic crosslinking of the molecular network.

The temporal evolution of the HHG is directly linked to the kinetics at which its constituent SDCs and CMH assemble into networks. The HHG initially solidifies due to the gelation of the mechanically rigid SDC network. It then forms a sturdier hydrogel over time

as the interpenetrating CMH molecular network becomes crosslinked by Ca^{2+} ions released *in situ* (Fig. 4c & d). The final value of G' of the HHG system is ~3× larger than that of the pure SDCs, in agreement with the mechanical data reported in Fig. 3. These material properties reveal controlled initial yield stresses and slow buildup of hydrogel elasticity over time. This makes them particularly suitable as 3D printable materials for making of intricate and sturdy hydrogel architectures.

3D printing with HHGs. The homocomposite approach allows precise control over the properties of the mixture in a way that enables 3D printing via extrusion, which has traditionally been challenging with hydrogel precursors. Notably, neither of the two components of the composite gel are viable as printing inks on their own. Pure SDC suspensions are mechanically stable upon extrusion and maintain their shape upon removal of an applied stress. However, they alone cannot be readily crosslinked produce a stiff elastic material (Supplementary Fig. 4). Conversely, non-crosslinked CMH solutions are unsuitable for extrusion additive printing because they slowly form solid gels by GDL-$CaCO_3$ crosslinking (Fig. 4b), a solidification process that requires time on the order of hours to days. By making a homocomposite ink using these two distinct forms of alginate, we present a new type of bespoke, extrudable hydrogel material in which the time-independent yield stress and solidification time can be tuned on demand. As the 3D printer applies a pressure drop that is greater than the yield stress of the HHGs, the extruded shape is preserved by the rapid gelation of the SDC network (Fig. 4c, Supplementary Video 1).

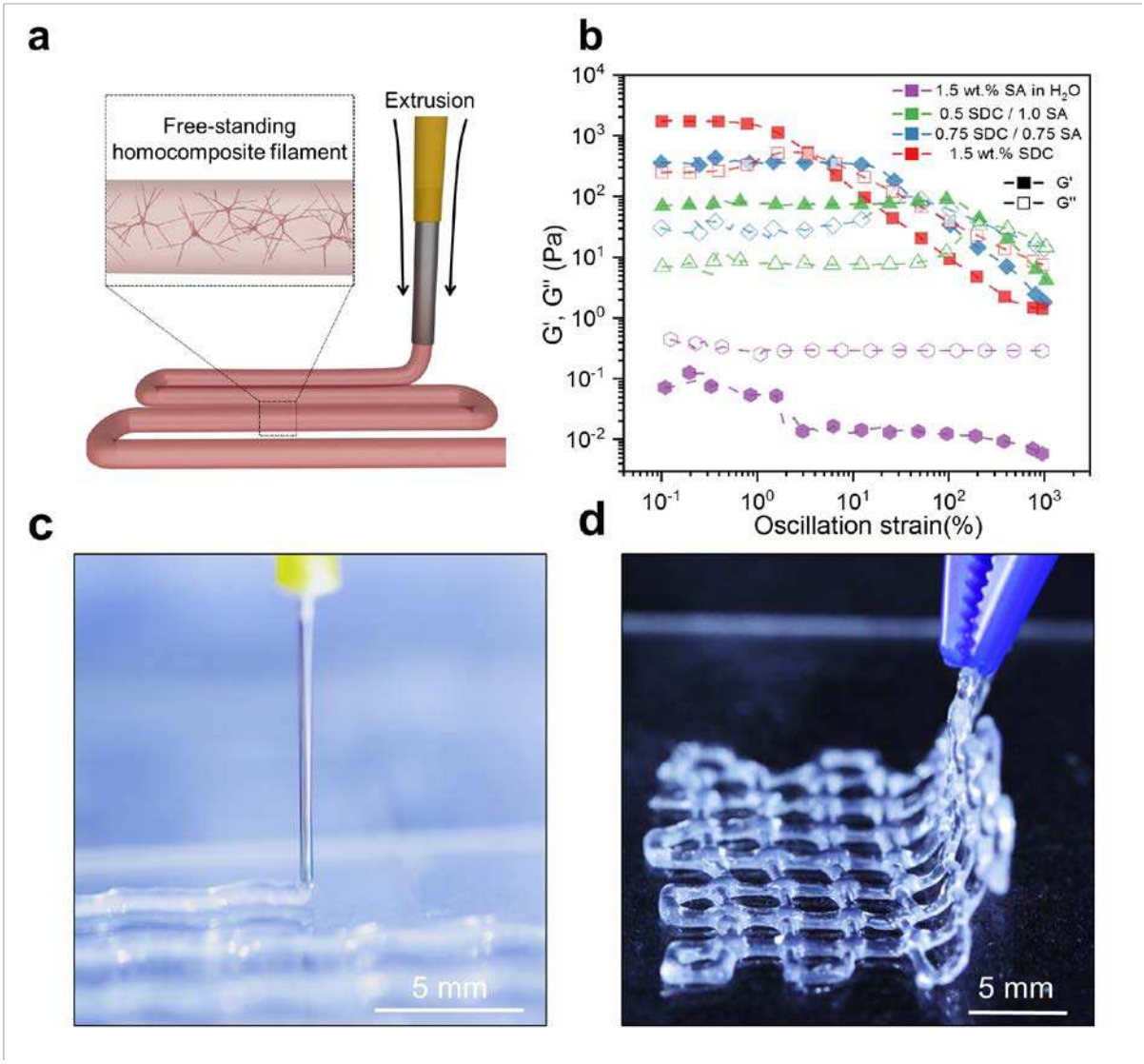

Fig. 5 | 3D Printing with homocomposite hydrogels. a Schematic illustration of 3D printing of SA SDC filled sodium alginate ink. **b** Complex modulus vs. stress curves for 1.5 total wt.% SA and SDC/SA HHG mixtures containing $CaCO_3$ nanoparticles, prior to GDL addition measured at 6.23 rad/s. **c** Picture of the 3D printed HHG ink (0.75 wt.% SDC, 0.75% CMH) during extrusion from a 25G tip and **d** removal of the equilibrated hydrogel design from the substrate. HHG formulations have the ability to flow upon extrusion, maintain their shape due to the colloidal yield stress, and result in a strongly self-reinforced structure following completion of the secondary ionic crosslinking reaction.

To demonstrate the extrudability and shapeability of such hydrogels combining colloidal and molecular networks, HHG formulations with total alginate concentration of 1.5 wt.% were loaded into a 3D printer operating by pressure-driven extrusion (Fig. 5a). The homocomposite systems were amenable to 3D printing in ambient conditions without necessitating a crosslinker bath or yield stress medium to maintain its shape. Notably, the *G'*

of 1500 Pa of pure SDC suspension is nearly four orders of magnitude larger than that of the CMH mixture at the same concentration prior to GDL addition (0.5 Pa, Fig. 5b).

The mixing of SDCs and CMHs results in the emergence of yield stress at all ratios tested. At small applied strains, the network remains a solid-like material due to the van der Waals interactions. As the strain increases beyond the yield point, the physical entanglements between the SDC fibrils are overcome and the yielded material can be extruded. Despite maximal HHG gel stiffness emerging at lower relative SDC/CMH ratios (Fig. 4c), HHG formulations with greater relative SDC contents produced more pristine filaments with improved filament layering (Supplementary Video 2). The maximum G* obtained at a 1/1 SDC/CMH ratio is consistent with the results of equilibrated 1.0 wt.% HHGs, which show a similar maximum G* at that ratio (Supplementary Fig. 5). The increased yield stresses of 1.5% SA HHGs enabled smooth and consistent HHGs extrusion for 3D printing.

The process of 3D printing of a homocomposite hydrogel by direct extrusion in air is demonstrated in Fig. 5c. The HHG formulation is extruded through a nozzle (25G, 0.26 mm ID) at 140 kPa and the shaped gel retains neatly its shape due its yield stress (≈ 80 Pa). Following molecular crosslinking and stiffening in 10-15 min, the printed hydrogel mesh could be readily removed from the substrate (Fig. 5d). Further adjustment of the relative concentrations of SA, SDCs, $CaCO_3$, and GDL allows the formulation of printable homocomposite hydrogels with tunable properties.

Discussion

We introduce a class of homocomposite hydrogels that are self-reinforced by a network of alginate SDCs interspersed within an alginate CMH network. The dispersed and adhesive nanofibrillar coronas of the SDCs lead to the formation of strong gels in SDC suspensions at very low volume fractions. They enable the formation of sturdy HHGs when interspersed in a continuous, molecular gel of the same biopolymer. The stiffness of the resulting HHG appears

to be governed by the synergistic interactions of the molecular alginate network and the colloidal-scale fibrillar SDC network. These HHGs are made using SA as a common polymer, but the principle can be applied to other hydrogels of natural or synthetic origin. The HHGs in this study demonstrate two distinctive emerging concepts that can guide materials design of new classes of hydrogels. First, the HHGs are stabilized by interpenetrating double networks at two very different length scales: molecular (nanometer scale) and colloidal (up to microscale). Second, due to the chemical uniformity of both networks, these hydrogels are ***both*** double network and homocomposite, which enables to adjust their unusual and potentially practically useful properties.

The fabrication of such designer materials is enabled by the ability of the SDCs to control media viscoelasticity and composite stiffness. The SDCs bring about rapid physical solidification due to van der Waals adherence between their nanofibrillar coronas. This allows extrudability and injectability that are key prerequisites for numerous applications of hydrogels. The HHGs thus present a solution to the problem that molecular alginates and other common gel precursors are poorly suited for extrusion shaping (such as in 3D printing and injection) because they lack initial yield stress and remain fluid for some time after extrusion.

While the alginate-alginate system demonstrates the advantages of homocomposite formulations, the potential of SDCs as viscoelastic modification and yield stress additives can be extended to a multitude of other systems. The SDCs are highly efficient as homocomposite fillers and their dispersion within other continuous polymer phases allows precise modulation of their viscoelasticity and composite stiffness at extremely low filler concentrations. The physical gelling of SDC as means of imparting immediate yield stress to a mixture that can be immediately 3D printed and subsequently builds up strength can also be applied in heterocomposite formulations as well. As an example, we constructed heterocomposite

formulations with a silicon matrix and polyvinyl alcohol SDCs that exhibit yield stress at extremely dilute SDC concentrations and form polydimethylsiloxane elastomer inks suitable for 3D printing by extrusion (Supplementary Fig. 6).

The SA HHG examples unveiled here have numerous potential applications such as biomedical 3D printing[32,60–62], soft robotics[3], food products with 3D printed edible structures[63], and haptic materials with unique mechanical responses[64]. They could also enhance the design of new green and sustainable materials made from biodegradable polymers. The most impactful feature of their structure is that the homocomposite colloidal-molecular double network enables independent tuning of chemical composition and material properties. This approach can be transcribed to other new classes of soft matter, whose functionality will be derived from their multi-scale network morphology, rather than their molecular composition. Overall, the SDCs emerge as a new class of soft colloids capable of tailoring the properties of many forthcoming liquid and solid composite materials.

Methods

Fabrication and characterization of SA SDCs

Alginic acid sodium salt (SA, Sigma, 120-190 kDa) was dissolved in distilled water (Millipore) at 3% (w/w). Following dissolution, the mixture was stored at 4ºC. To fabricate SA SDCs, a colloidal high-shear mixer (IKA Magic Lab) was first filled with 500 mL of 13.6 mM calcium ion precipitation medium ($CaCl_2$•$2H_2O$, Sigma-Aldrich). A volume of 20 mL of 3 wt.% SA solution was injected directly into the shear zone of the device at 20,000 rpm using a machined injection attachment, where the SDCs form nearly instantaneously via ionic precipitation and are left suspended in the precipitation medium. SDC suspensions were centrifuged for 3 minutes at 3.0 rcf, resulting in the formation of a concentrated SDC pellet. The compacted SDCs were then re-suspended to 8× their pellet volume in distilled water

using a Vortex mixer. This process was repeated 5× to remove any remaining ions from the suspension. Following particle washing, the SDCs were centrifuged and diluted to their desired concentration. Particle morphologies were visualized using optical microscopy (BX-61 Olympus) and field emission scanning electron microscopy (FEI Verios 460L scanning electron microscope). Images were processed using ImageJ to adjust brightness and contrast.

Making of molecularly crosslinked SA hydrogels

Conventional CMHs were prepared by the addition of 0.1 wt.% $CaCO_3$ nanoparticles (NPs, American Elements®) and 28.14 mM solution of D-Gluconic acid δ-lactone (GDL, Sigma-Aldrich) to an aqueous SA solution as described previously[58]. Upon dissolution in water and addition to the alginate mixture, GDL slowly hydrolyzes, reducing the pH and gradually ionizing the $CaCO_3$ NPs to release Ca^{2+} crosslinker ions[59]. This is preferred over the addition of instantly soluble Ca salt (like $CaCl_2$) since it allows more homogeneous SA gel formation.

Preparation of alginate homocomposite hydrogels:

Alginate molecular/SDC gels were made by first preparing stock solutions of 3.0 wt.% SA in water, mixed with 0.30 wt.% $CaCO_3$ nanoparticles, 1.38 wt.% SA SDCs in water and stirred thoroughly to reach the desired concentrations. To induce homogenous gelation, a bolus of freshly prepared 20 wt.% D-(+)-gluconic acid δ-lactone in water was added to the mixture at a ratio of 5/1 (GDL/$CaCO_3$ w/w) and homogenized using a Vortex device. All gels were given 2 hours to complete crosslinking prior to characterization. The final concentrations of each constituent of HHGs are shown in Table 1.

Rheological and tensile characterization of suspensions and hydrogels:

The viscoelastic properties of the SDC suspensions and HHGs were evaluated using a rheometer (Discovery HR-2, TA Instruments) equipped with a sandblasted plate and plate geometry (40 mm diameter and 0.8 mm gap size) with the temperature maintained at 25°C for all experiments. Small amplitude oscillatory frequency sweeps were performed within the

linear viscoelastic regime. Amplitude sweeps were performed between 0.1 and 1000% strain at a frequency of 6.23 rad/s and time sweeps were performed at a frequency of 1 rad/s with 1% strain. The tensile properties of the gels were determined using a common testing machine (Instron 5943) with samples of 1.5 mm thickness, 44 mm width, 10 mm length, and a 5 $cm \cdot min^{-1}$ crosshead speed. Laser-cut acrylic molds were used to shape hydrogels during equilibration and laser-cut acrylic grips were used for tensile analysis to avoid directly gripping the hydrogel sample. A thin layer of cyanoacrylate adhesive (Gorilla Glue Gel) was used for chemically bonding the gel to the grips to ensure that slippage did not occur during extension (Supplementary Fig. 7).

Data availability statement

Data available on request from the authors.

References

1. Sun, J. Y. *et al.* Highly stretchable and tough hydrogels. *Nature* **489**, 133–136 (2013).
2. Pääkko, M. *et al.* Enzymatic hydrolysis combined with mechanical shearing and high-pressure homogenization for nanoscale cellulose fibrils and strong gels. *Biomacromolecules* **8**, 1934–1941 (2007).
3. Palleau, E., Morales, D., Dickey, M. D. & Velev, O. D. Reversible patterning and actuation of hydrogels by electrically assisted ionoprinting. *Nat. Commun.* **4**, 1–7 (2013).
4. Haque, M. A., Kurokawa, T., Kamita, G., Yue, Y. & Gong, J. P. Rapid and reversible tuning of structural color of a hydrogel over the entire visible spectrum by mechanical stimulation. *Chem. Mater.* **23**, 5200–5207 (2011).
5. Zhao, X. *et al.* Active scaffolds for on-demand drug and cell delivery. *Proc. Natl. Acad. Sci.* **108**, 67–72 (2011).
6. Li, J. *et al.* Tough adhesives for diverse wet surfaces. *Science* **357**, 378–381 (2017).
7. Lee, K. Y. & Mooney, D. J. Alginate: Properties and biomedical applications. *Prog. Polym. Sci.* **37**, 106–126 (2012).
8. Yuk, H. *et al.* Hydraulic hydrogel actuators and robots optically and sonically camouflaged in water. *Nat. Commun.* **8**, 1–12 (2017).
9. Langer, R. Drug delivery and targeting. *Nature* **392**, 5–10 (1998).
10. Cayre, O. J., Suk, T. C. & Velev, O. D. Polyelectrolyte diode: Nonlinear current response of a junction between aqueous ionic gels. *J. Am. Chem. Soc.* **129**, 10801–10806 (2007).
11. Zhao, X. Multi-scale multi-mechanism design of tough hydrogels: Building dissipation into stretchy networks. *Soft Matter* **10**, 672–687 (2014).
12. Hong, S. *et al.* 3d printing of highly stretchable and tough hydrogels into complex,

cellularized structures. *Adv. Mater.* 4035–4040 (2015) doi:10.1002/adma.201501099.
13. Takahashi, R. *et al.* Creating stiff, tough, and functional hydrogel composites with low-melting-point alloys. *Adv. Mater.* **30**, 1–7 (2018).
14. Hu, J. *et al.* Microgel-reinforced hydrogel films with high mechanical strength and their visible mesoscale fracture structure. *Macromolecules* **44**, 7775–7781 (2011).
15. Creton, C. 50th anniversary perspective: Networks and gels: soft but dynamic and tough. *Macromolecules* **50**, 8297–8316 (2017).
16. Gong, J. P., Katsuyama, Y., Kurokawa, T. & Osada, Y. Double-network hydrogels with extremely high mechanical strength. *Adv. Mater.* **15**, 1155–1158 (2003).
17. Takahashi, R. *et al.* Tough particle-based double network hydrogels for functional solid surface coatings. *Adv. Mater. Interfaces* **5**, 1–10 (2018).
18. Illeperuma, W. R. K., Sun, J. Y., Suo, Z. & Vlassak, J. J. Fiber-reinforced tough hydrogels. *Extrem. Mech. Lett.* **1**, 90–96 (2014).
19. Lee, J. & Lee, K. Y. Injectable microsphere/hydrogel combination systems for localized protein delivery. *Macromol. Biosci.* **9**, 671–676 (2009).
20. Bakarich, S. E., Gorkin, R. & Spinks, M. Three-dimensional printing fiber reinforced hydrogel composites. *ACS Appl. Mater. Interfaces* (2014) doi:10.1021/am503878d.
21. Lin, W., Fan, W., Marcellan, A., Hourdet, D. & Creton, C. Large strain and fracture properties of poly (dimethylacrylamide)/ silica hybrid hydrogels. *Macromolecules* 2554–2563 (2010) doi:10.1021/ma901937r.
22. Thoniyot, P., Tan, M. J., Karim, A. A., Young, D. J. & Loh, X. J. Nanoparticle–hydrogel composites: concept, design, and applications of these promising, multi-functional materials. *Adv. Sci.* **2**, 1400010 (2015).
23. Dong, Q. *et al.* A new bioactive polylactide-based composite with high mechanical strength. *Colloids Surfaces A Physicochem. Eng. Asp.* **457**, 256–262 (2014).
24. Tonsomboon, K., Butcher, A. L. & Oyen, M. L. Strong and tough nanofibrous hydrogel composites based on biomimetic principles. *Mater. Sci. Eng. C* **72**, 220–227 (2017).
25. Kmetty, Á., Bárány, T. & Karger-Kocsis, J. Self-reinforced polymeric materials: A review. *Prog. Polym. Sci.* **35**, 1288–1310 (2010).
26. Al-Saleh, M. H. & Sundararaj, U. Review of the mechanical properties of carbon nanofiber/polymer composites. *Compos. Part A Appl. Sci. Manuf.* **42**, 2126–2142 (2011).
27. Jenkins, T. L. & Little, D. Synthetic scaffolds for musculoskeletal tissue engineering: cellular responses to fiber parameters. *Regen. Med.* **4**, 1–14 (2019).
28. Roohani-Esfahani, S. I., Newman, P. & Zreiqat, H. Design and fabrication of 3D printed scaffolds with a mechanical strength comparable to cortical bone to repair large bone defects. *Sci. Rep.* **6**, 1–8 (2016).
29. Banerjee, H., Suhail, M. & Ren, H. Hydrogel actuators and sensors for biomedical soft robots: brief overview with impending challenges. *Biomimetics* **3**, 15 (2018).
30. Capiati, N. J. & Porter, R. S. The concept of one polymer composites modelled with high density polyethylene. *J. Mater. Sci.* **10**, 1671–1677 (1975).
31. Shesan, O. J., Stephen, A. C., Chioma, A. G. & Neerish, Revaprasadu and Rotimi, S. E. Fiber-matrix relationship for composites preparation. *Composites from Renewable and Sustainable Materials* 1–30 (IntechOpen, 2019). doi:10.5772/57353.
32. Roh, S., Parekh, D. P., Bharti, B., Stoyanov, S. D. & Velev, O. D. 3D printing by multiphase silicone/water capillary inks. *Adv. Mater.* **29**, 1–7 (2017).
33. Roh, S. & Velev, O. D. Nanomaterials fabrication by interfacial templating and capillary engineering in multiphasic liquids. *AIChE J.* **64**, (2018).
34. Roh, S. C., Kim, J. & Kim, C. K. Characteristics of nylon 6,6/nylon 6,6 grafted multi-walled carbon nanotube composites fabricated by reactive extrusion. *Carbon N. Y.* **60**,

317–325 (2013).
35. Kovačević, V., Lučić, S. & Cerovečki, Ž. Influence of filler surface pre-treatment on the mechanical properties of composites. *Int. J. Adhes. Adhes.* **17**, 239–245 (1997).
36. Fu, S. Y., Feng, X. Q., Lauke, B. & Mai, Y. W. Effects of particle size, particle/matrix interface adhesion and particle loading on mechanical properties of particulate-polymer composites. *Compos. Part B Eng.* **39**, 933–961 (2008).
37. Izer, A. & Bárány, T. Hot consolidated all-PP composites from textile fabrics composed of isotactic PP filaments with different degrees of orientation. *Express Polym. Lett.* **1**, 790–796 (2007).
38. Matabola, K. P., De Vries, A. R., Moolman, F. S. & Luyt, A. S. Single polymer composites: A review. *J. Mater. Sci.* **44**, 6213–6222 (2009).
39. Fakirov, S. Nano- and microfibrillar single-polymer composites: A review. *Macromol. Mater. Eng.* **298**, 9–32 (2013).
40. Karger-Kocsis, J. & Bárány, T. Single-polymer composites (SPCs): Status and future trends. *Compos. Sci. Technol.* **92**, 77–94 (2014).
41. Roh, S., Williams, A. H., Bang, R. S., Stoyanov, S. D. & Velev, O. D. Soft dendritic microparticles with unusual adhesion and structuring properties. *Nat. Mater.* **18**, 1315–1320 (2019).
42. Asteriadi, A. *et al.* Molecular control of the viscosity of model dendritically branched polystyrene solutions: From polymeric to colloidal behavior. *Macromolecules* **37**, 1016–1022 (2004).
43. Harreis, H. M., Likos, C. N. & Ballauff, M. Can dendrimers be viewed as compact colloids? A simulation study of the fluctuations in a dendrimer of fourth generation. *J. Chem. Phys.* **118**, 1979–1988 (2003).
44. Raghavan, S. R. & Douglas, J. F. The conundrum of gel formation by molecular nanofibers, wormlike micelles, and filamentous proteins: Gelation without cross-links? *Soft Matter* **8**, 8539–8546 (2012).
45. Cui, W. *et al.* Fiber-reinforced viscoelastomers show extraordinary crack resistance that exceeds metals. *Adv. Mater.* **32**, 1–9 (2020).
46. Kizilova, N. Nature inspired optimal design of heat conveying networks for advanced fiber-reinforced composites. *J. Therm. Eng.* **1**, 636–646 (2015).
47. Laubie, H., Radjai, F., Pellenq, R. & Ulm, F. J. Stress transmission and failure in disordered porous media. *Phys. Rev. Lett.* **119**, (2017).
48. Fang, M., Dong, G., Wei, R. & Ho, J. C. Hierarchical nanostructures: Design for sustainable water splitting. *Adv. Energy Mater.* **7**, 1–25 (2017).
49. Masselter, T. *et al.* Biomimetic optimisation of branched fibre-reinforced composites in engineering by detailed analyses of biological concept generators. *Bioinspiration and Biomimetics* **11**, (2016).
50. Perazzo, A., Nunes, J. K., Guido, S. & Stone, H. A. Flow-induced gelation of microfiber suspensions. *Proc. Natl. Acad. Sci. U. S. A.* **114**, E8557–E8564 (2017).
51. Hsiao, L. C., Newman, R. S., Glotzer, S. C. & Solomon, M. J. Role of isostaticity and load-bearing microstructure in the elasticity of yielded colloidal gels. *Proc. Natl. Acad. Sci. U. S. A.* **109**, 16029–16034 (2012).
52. Moghimi, E., Jacob, A. R., Koumakis, N. & Petekidis, G. Colloidal gels tuned by oscillatory shear. *Soft Matter* **13**, 2371–2383 (2017).
53. Chambon, F. & Winter, H. H. Linear Viscoelasticity at the gel point of a crosslinking pdms with imbalanced stoichiometry. *J. Rheol. (N. Y. N. Y).* **31**, 683–697 (1987).
54. Autumn, K. & Peattie, A. M. Mechanisms of adhesion in geckos. *Integr. Comp. Biol.* **42**, 1081–1090 (2002).
55. Fernández Farrés, I., Douaire, M. & Norton, I. T. Rheology and tribological properties of Ca-alginate fluid gels produced by diffusion-controlled method. *Food Hydrocoll.* **32**,

115–122 (2013).
56. Fernández Farrés, I., Moakes, R. J. A. & Norton, I. T. Designing biopolymer fluid gels: A microstructural approach. *Food Hydrocoll.* **42**, 362–372 (2014).
57. Fernández Farrés, I. & Norton, I. T. Formation kinetics and rheology of alginate fluid gels produced by in-situ calcium release. *Food Hydrocoll.* **40**, 76–84 (2014).
58. Kuo, C. K. & Ma, P. X. Ionically crosslinked alginate hydrogels as scaffolds for tissue engineering: part 1. Structure, gelation rate and mechanical properties. *Biomaterials* **22**, 511–21 (2001).
59. Jang, J. *et al.* Effects of alginate hydrogel cross-linking density on mechanical and biological behaviors for tissue engineering. *J. Mech. Behav. Biomed. Mater.* **37**, 69–77 (2014).
60. Minas, C., Carnelli, D., Tervoort, E. & Studart, A. R. 3D printing of emulsions and foams into hierarchical porous ceramics. *Adv. Mater.* **28**, 9993–9999 (2016).
61. Mueller, J., Raney, J. R., Shea, K. & Lewis, J. A. Architected lattices with high stiffness and toughness via multicore–shell 3D printing. *Adv. Mater.* **30**, 1–8 (2018).
62. Kass, L., Cardenas-Vasquez, E. D. & Hsiao, L. C. Composite double network hydrogels with thermoresponsive colloidal nanoemulsions. *AIChE J.* **65**, 1–8 (2019).
63. Shewan, H. M. & Stokes, J. R. Review of techniques to manufacture micro-hydrogel particles for the food industry and their applications. *J. Food Eng.* **119**, 781–792 (2013).
64. Peng, Y., Serfass, C. M., Hill, C. N. & Hsiao, L. C. Lubricated friction of textured soft substrates. *arXiv Prepr.* (2019).

Acknowledgements

This study was supported by a grant from US National Science Foundation, no. CMMI-1825476. L.C.H. and A. R. J. are supported by a grant from the National Science Foundation (NSF CBET-1804462). We thank Dr. Michael Dickey for the use of his instrumentation for mechanical characterization of hydrogel samples.

Author contributions

A.W., S.R., and O.V. initiated this work with A.W. and S.R. contributing equally. Experiments and analysis were completed by A.W., A.J., and S.R. This work was advised by O.V., S.S. and L.H. A.W., S.R., A.J., L.H., and O.V. wrote the manuscript.

Competing interests

The authors declare no competing financial interests.

Materials & Correspondence

Corresponding author: odvelev@ncsu.edu

Table 1. Equilibrium compositions of SA CMH/SDC HHGs in [wt.%].

SA CMH/SDC Homocomposite Compositions (wt.%)

wt.% SDC	**0.000**	**0.125**	**0.250**	**0.500**	**0.750**	**1.000**
wt.% CMH	**1.000**	**0.875**	**0.750**	**0.500**	**0.250**	**0.000**
$CaCO_3$ (wt.%)	0.100	0.0875	0.075	0.050	0.025	0.000
Total [Ca^{2+}] (wt.%)	0.040	0.061	0.082	0.124	0.166	0.208
[GDL] (wt.%)	0.500	0.439	0.378	0.250	0.125	0.000

Figures

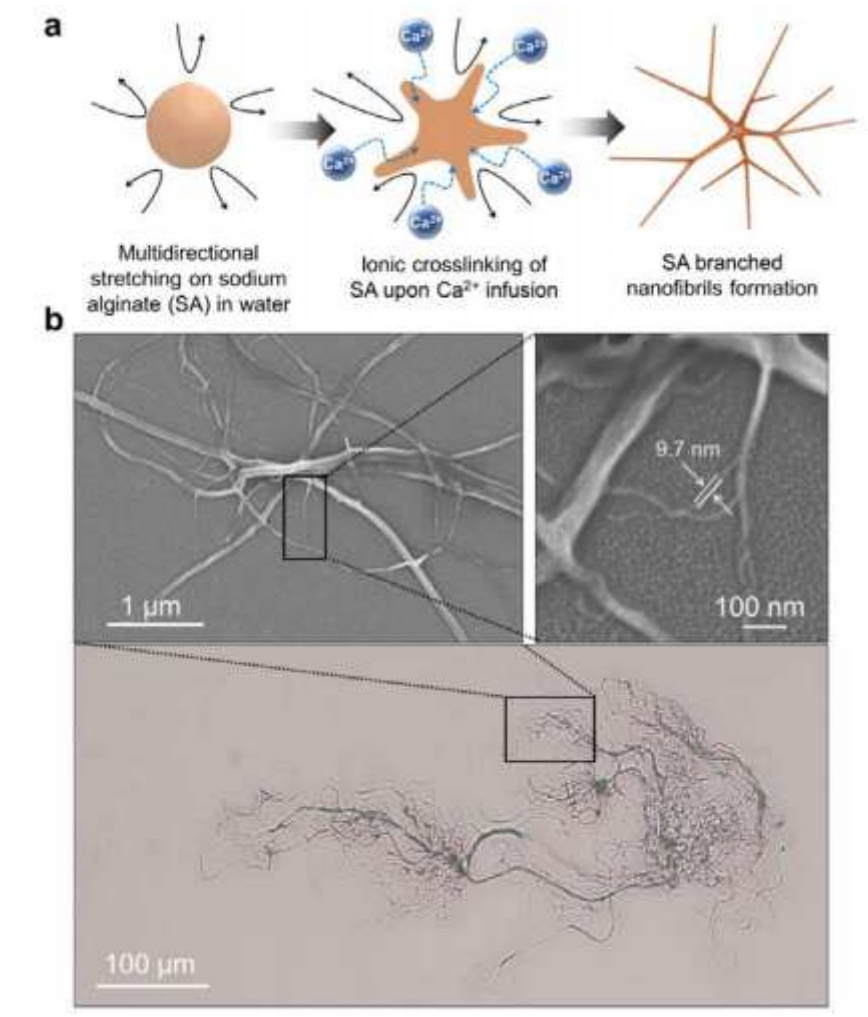

Figure 1

Turbulent shear-driven precipitation and morphology of a sodium alginate soft dendritic colloid. a Schematic of the SA SDC formation process by precipitation in a turbulent medium. b Optical microscopy and field emission scanning electron microscopy (FE-SEM) images of sodium alginate soft dendritic colloids. These images illustrate the hierarchical fibrillar morphology of the SDCs, which leads to high exclusion volume, strong van der Waals adhesivity and high propensity for gelation.

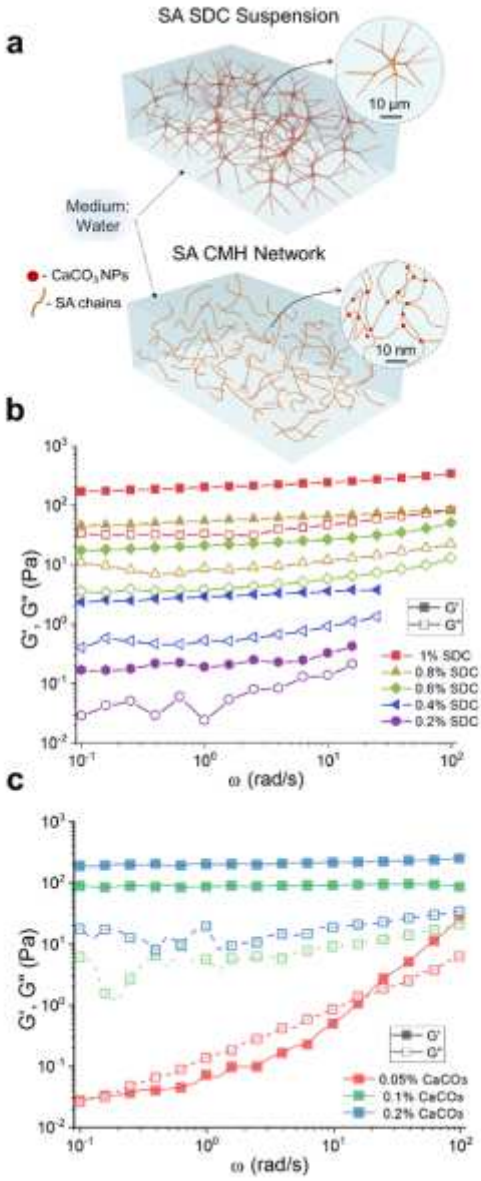

Figure 2

Linear viscoelasticity and yield stress of SA SDC suspensions and molecular gels. a Schematic that compares the gelation mode of a viscoelastic suspension of SDCs and that of a crosslinked SA molecular hydrogel (CMH). Note the different length scales of the networks. b Frequency sweeps indicating the storage modulus (G', filled) and loss modulus (G", unfilled) of SA SDCs in aqueous suspensions. c Frequency sweeps indicating the storage modulus (G', filled) and loss modulus (G", unfilled) of 1.0% SA CMHs with 0.05%, 0.1% and 0.2% CaCO3 nanoparticles and 28.14 mM GDL following 2 hours for equilibration.

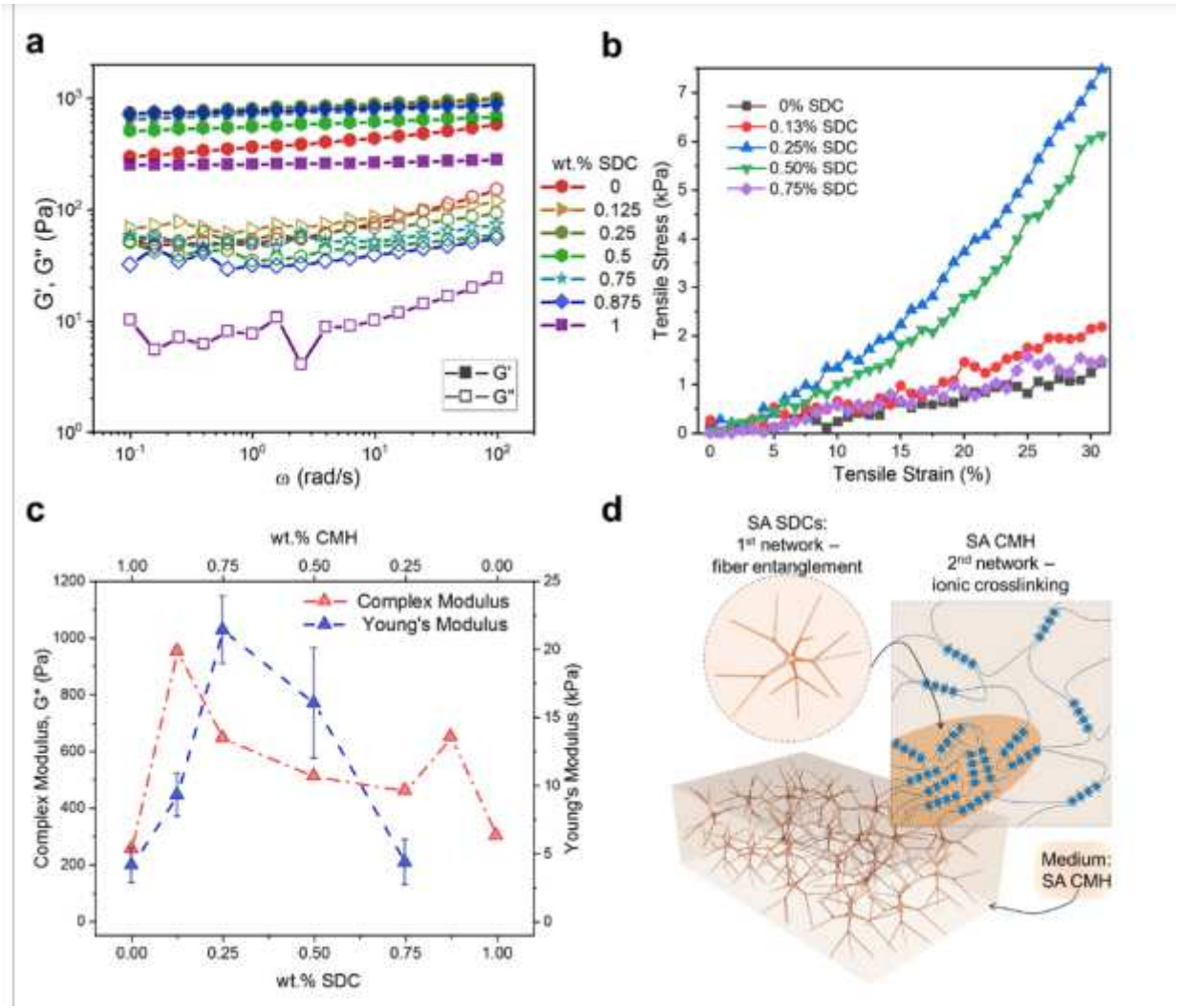

Figure 3

Mechanical properties of SA homocomposite gels. a Frequency sweeps of 1.0% HHGs of varying SDC concentrations (n=2). b Representative stress-strain curves for various HHGs. c Rheological (□, n=2) and tensile (□, n=5) properties of various SDC/CMH HHGs. Total alginate concentration is maintained at 1.0 wt.% for all data. d Schematic of the hierarchical interactions between the colloidal and molecular alginate networks in HHGs. These results demonstrate the structural synergism of the double SDC and CMH networks within HHGs resulting in controllable and self-reinforced high composite stiffness.

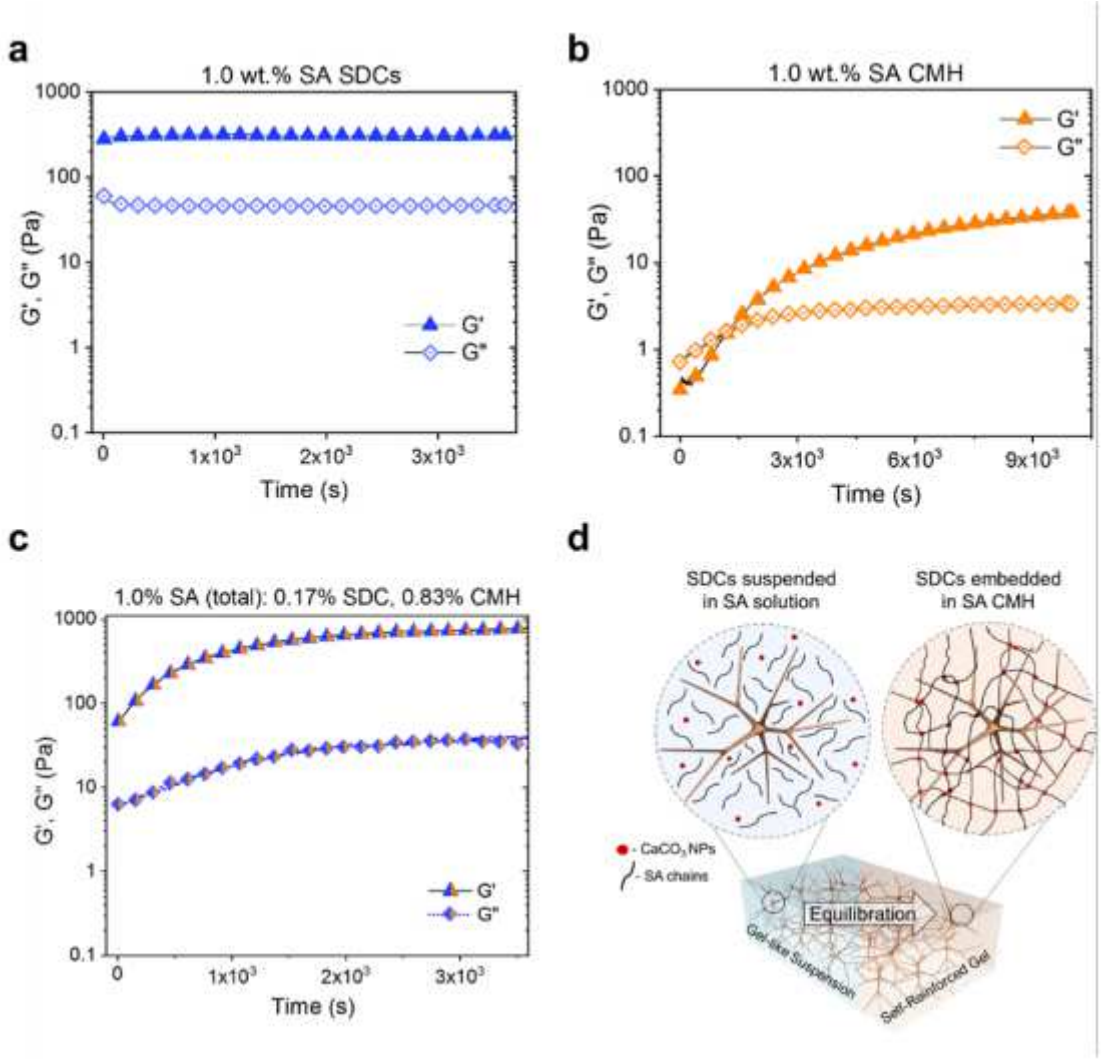

Figure 4

Time-dependent gelation of SA SDC suspensions, SA CMHs, and SA HHGs. Time sweeps indicating G' and G" (1 rad/s, 1% strain) of a 1.0 % SA SDC suspension in water, b 1.0% SA CMH following GDL addition and c 1.0% total SA (0.17% SDC, 0.83% CMH) HHG following GDL addition. d Schematic showing the time-dependent transition of a HHG from a colloidal gel to a selfreinforced homocomposite via CMH crosslinking. HHG formulations show immediate, elastic-solid behavior from the colloidal network and further stiffen with the ionic crosslinking of the molecular network.

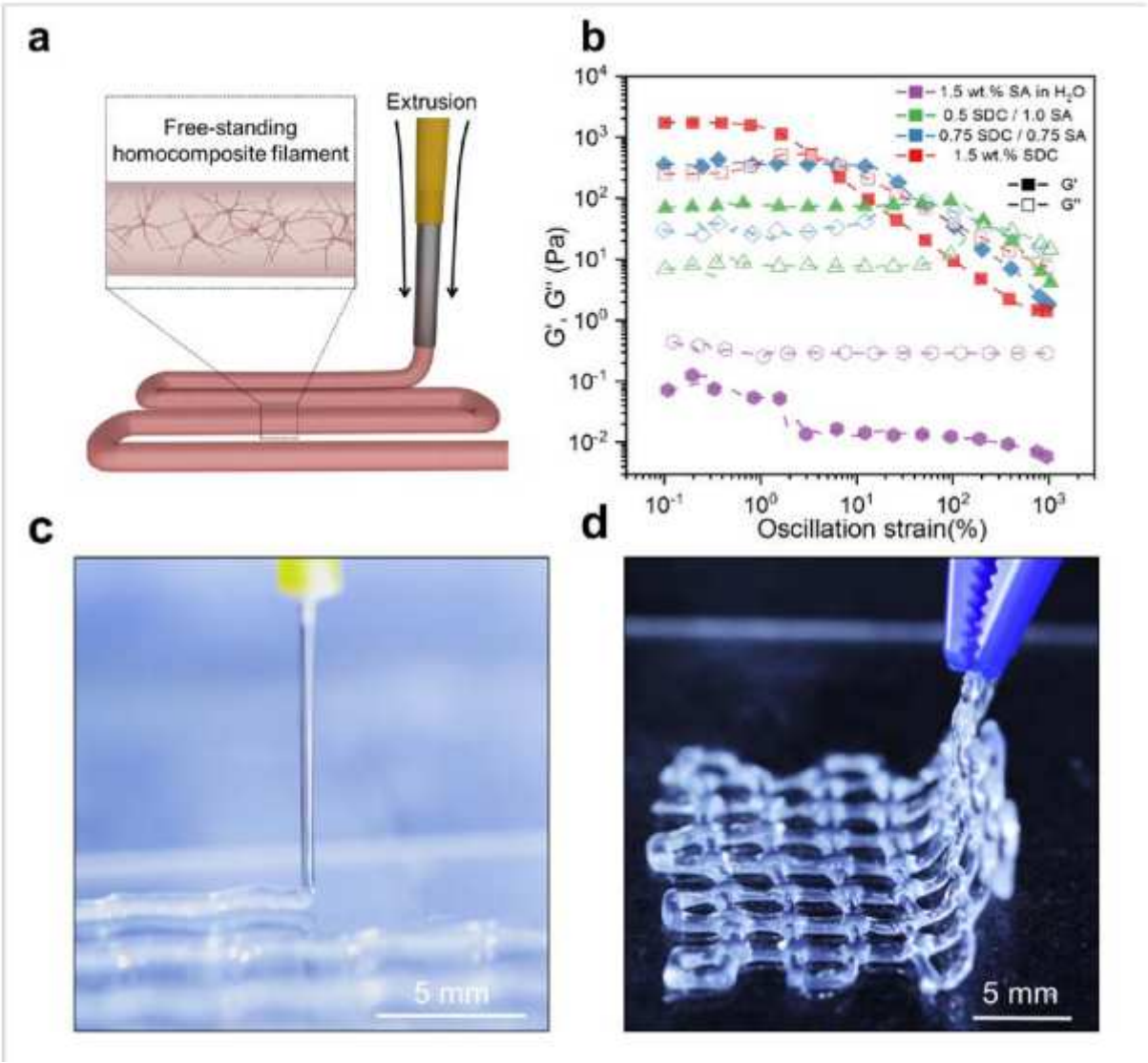

Figure 5

3D Printing with homocomposite hydrogels. a Schematic illustration of 3D printing of SA SDC filled sodium alginate ink. b Complex modulus vs. stress curves for 1.5 total wt.% SA and SDC/SA HHG mixtures containing CaCO3 nanoparticles, prior to GDL addition measured at 6.23 rad/s. c Picture of the 3D printed HHG ink (0.75 wt.% SDC, 0.75% CMH) during extrusion from a 25G tip and d removal of the equilibrated hydrogel design from the substrate. HHG formulations have the ability to flow upon extrusion, maintain their shape due to the colloidal yield stress, and result in a strongly selfreinforced structure following completion of the secondary ionic crosslinking reaction.

Supplementary Files

This is a list of supplementary files associated with this preprint. Click to download.

- SISDCHomocompositeHydrogelsNatComFinal.pdf
- SupplementaryVideo1.mp4

- SupplementaryVideo2.mp4